

Trends and variability of sea ice in Baffin Bay and Davis Strait, 1953–2001

Harry L. Stern & Mads Peter Heide-Jørgensen



The extent and duration of sea ice in Baffin Bay and Davis Strait has a major impact on the timing and strength of the marine production along West Greenland. The advance and retreat of the sea ice follows a predictable pattern, with maximum extent typically in March. We examine the area of sea ice in March in three overlapping study regions centred on Disko Bay on the west coast of Greenland. Sea ice concentration estimates derived from satellite passive microwave data are available for the years 1979–2001. We extend the record back in time by digitizing ice charts from the Danish Meteorological Institute, 1953–1981. There is reasonable agreement between the chart data and the satellite data during the three years of overlap: 1979–1981. We find a significant increasing trend in sea ice for the 49-year period (1953–2001) for the study regions that extend into Davis Strait and Baffin Bay. The cyclical nature of the wintertime ice area is also evident, with a period of about 8 to 9 years. Correlation of the winter sea ice concentration with the winter North Atlantic Oscillation (NAO) index shows moderately high values in Baffin Bay. The correlation of ice concentration with the previous winter's NAO is high in Davis Strait and suggests that next winter's ice conditions can be predicted to some extent by this winter's NAO index.

H. L. Stern, Polar Science Center, Applied Physics Laboratory, University of Washington, 1013 NE 40th St., Seattle, WA 98105-6698, USA, harry@apl.washington.edu; M. P. Heide-Jørgensen, Greenland Institute of Natural Resources c/o National Marine Mammal Laboratory, 7600 Sand Point Way NE, Seattle, WA 98115, USA.

The southern part of Baffin Bay and Davis Strait is characterized by very variable oceanographic conditions along the west coast of Greenland and more stable conditions along the east coast of Baffin Island. The Irminger Current, a side branch of the North Atlantic Current, brings warm and saline water of Atlantic origin northward along the west coast of Greenland. From the Arctic Ocean, water is driven southward through the Canadian Archipelago and into Baffin Bay, where it flows south along the east coast of Baffin Island and eventually becomes the Labrador Current. The strength of these currents as well as atmospheric forcing determines the extent and development of sea ice in southern Baffin Bay

and Davis Strait.

At the northern end of Baffin Bay, the North Water (NOW) Polynya is a persistent feature in winter and spring. An ice bridge forms across Nares Strait, blocking the southward flow of pack ice. South of the ice bridge, wind and currents drive newly forming sea ice southward into Baffin Bay, maintaining the polynya. A recent treatment of the circulation is given by Melling et al. (2001). Whether or not the ice bridge and polynya form, there is southward transport of sea ice into Baffin Bay during winter—either old pack ice or new polynya ice. This affects the mix of ice types in the northern part of the bay. Sea ice also forms in place within the bay.

The annual development of sea ice in Baffin Bay and Davis Strait, the so-called “West Ice”, starts in late autumn and continues through February and March, after which the ice recedes to the west and disappears almost completely in summer. Occasionally the ice will persist during summer in central Baffin Bay. At the peak of winter the West Ice usually reaches the west coast of Greenland north of 68°N. South of 68°N the West Ice turns westward, creating open water along the coast and a clear ice edge in Davis Strait.

Parkinson et al. (1999) found a trend in the wintertime sea ice extent of +7.5% per decade for 1979–1996 for the region encompassing Baffin Bay, Davis Strait and the Labrador Sea, based on satellite-derived sea ice concentration from passive microwave sensors. This was in contrast to an overall decrease of –2.2% per decade for the Northern Hemisphere. Deser et al. (2000) also noted an increasing ice cover west of Greenland for 1958–1997, based on a principal component analysis of the Northern Hemisphere wintertime sea ice concentration anomalies. The wintertime surface air temperature shows a trend of –2°C per decade for 1979–1997 along the west coast of Greenland north of 69°N, but a warming in the other seasons of +3°C per decade south of 69°N (Rigor et al. 2000). These regional changes in ice extent and air temperature are probably linked to the North Atlantic Oscillation (NAO)—the normalized difference in surface atmospheric pressure between Portugal and Iceland (Hurrell 1995).

Locally in West Greenland it has been observed that shrimp trawlers, operating in an area west of Disko Bay (between 68° and 70°N and west of 53° 30' W), have changed their average trawling positions for January through April to a more south-eastern position during the period 1977 to 1999 (Heide-Jørgensen, unpubl. data). This is an effect of increasing ice coverage in the north-western part of the area. The change in trawling activity is not caused by a change in shrimp abundance since the area where the main part of trawling occurs remains unchanged.

Weekly ice charts for March (the month of maximum ice extent) from 1972 through 1994 show that Davis Strait and the Labrador Sea are the most variable regions in the Northern Hemisphere (EWG 2000). Furthermore, predictions of Northern Hemisphere sea ice extent in March from five coupled atmosphere–ocean–sea ice models show that the largest disagreements

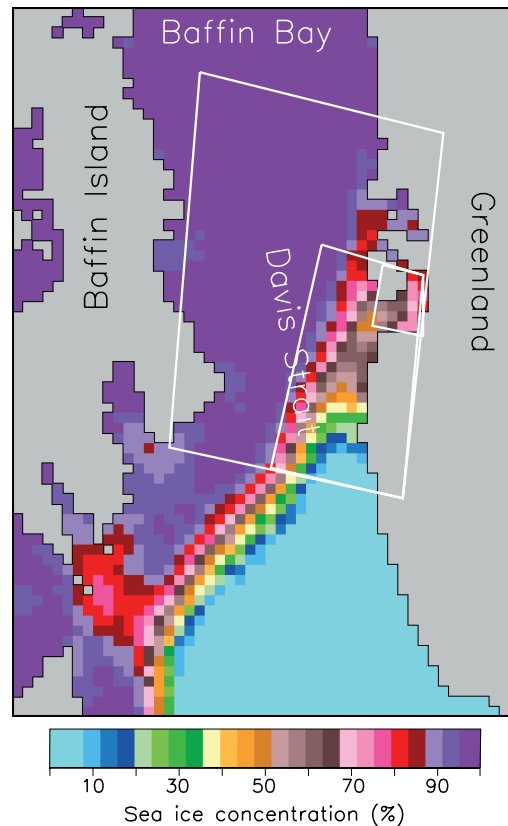


Fig. 1. The three overlapping study regions (white outlines) superimposed on the sea ice concentration from passive microwave satellite data for March 1979. The large study region extends from 65 to 73°N and from Greenland to Baffin Island. The medium study region extends from 65 to 70°N and halfway across Davis Strait. The small study region is centred on Disko Bay. The pixels in the sea ice concentration grid have a nominal size of 25 × 25 km and are clearly visible as discrete blocks. This is a 50 × 70-pixel subsection of the full 304 × 448 grid for the Northern Hemisphere.

between models are in Davis Strait and the Labrador Sea (J. Walsh, pers. comm.). These observations, together with the apparent positive trend in sea ice noted above, opposite to that of the hemisphere, warrant further study of the ice conditions in West Greenland. We examine the area of sea ice in March in three study regions using satellite-based passive microwave data (1979–2001), and chart data (1953–1981) from the Danish Meteorological Institute. The combined 49-year record shows a positive trend in sea ice in West Greenland. Links with the NAO are explored, with the objective of predicting future ice conditions in West Greenland.

Data sets

Study regions

The three overlapping study regions are shown in Fig. 1. The large region extends from 65 to 73° N and covers the waters between Greenland and Baffin Island. The medium region is focused on the West Greenland coast between 65 and 70° N. It covers the shear zone where the open water meets the Baffin Bay pack ice. The small region covers Disko Bay, an important fishing ground.

Satellite data

We use two data sets of monthly gridded sea ice concentration derived from passive microwave sensors. The first data set (October 1978 through December 1999) includes both the Scanning Multichannel Microwave Radiometer (SMMR, 1978–1987) and the Special Sensor Microwave Imager (SSMI, on various satellites since 1987). The second data set includes only SSMI from the F13 satellite (May 1995 to the present). Both data sets are derived using the Bootstrap algorithm for sea ice concentration (Comiso 1995), and are available from the National Snow and Ice Data Center (NSIDC). Each sea ice concentration grid for the Northern Hemisphere is 304×448 pixels and is mapped to a polar stereographic projection (true at 70° N) with a nominal pixel size of 25×25 km. Figure 1 shows a 50×70 pixel subsection centred on the three study regions. The areas of the regions (excluding land) are 439 000 km² (707 pixels), 118 000 km² (192 pixels), and 12 400 km² (20 pixels).

We use the sea ice concentration for March of each year, typically the month with the largest concentration in our regions of interest. We compute an area-weighted average over all pixels in a study region to get the mean ice concentration in that region for March. (Pixel areas vary slightly with latitude due to the map projection.) Thus the monthly estimates of ice concentration in each study region involve spatial and temporal averaging. The error in the daily ice concentration at each pixel is 5–10% according to documentation from NSIDC. Spatially averaging over a large number of pixels, as we do, greatly reduces the error standard deviation, although it does not reduce any systematic bias. Temporal variability within March is very low. Using daily values of ice concentration averaged over each study region, we

find typical standard deviations within March to be about 3–8% of the mean ice concentration.

Passive microwave data from the Electrically Scanning Microwave Radiometer (ESMR) on the Nimbus 5 satellite (1973–76) were also used to produce estimates of sea ice concentration, which are available from NSIDC. We examined this data set but did not use it, because the lack of overlap with SMMR makes cross-calibration too uncertain.

Chart data

From 1952 to 1981 the Danish Meteorological Institute (DMI) in Copenhagen published an annual volume called *The ice conditions in the Greenland waters*. Each volume contains maps of the ice concentration at the end of each month. Different types of shading denote ranges of ice concentration (in tenths), as in Fig. 2. Data for the charts came from ship and aircraft observations, land-based observations and (in later years) satellite images. The charts apparently evolved in three stages: 1952–56 charts have coarse resolution; 1957–1964 charts have better resolution, but sometimes with large areas of missing information; and 1967–1981 charts are as in Fig. 2, without areas of missing information (presumably filled by interpolation). We scanned the charts for March of each year, with the following exceptions: for 1952 (small region), 1953, 1955 and 1956 we had to use April; for 1952 (medium and large regions), 1954 and 1959 there was too much missing information in our regions of interest, so we excluded them; 1965 and 1966 were not available. Thus the chart data consists of April 1952 (small region only), 1953, 1955–56; and March 1957–58, 1960–64, 1967–1981. For each scanned chart, 15 tie points at known latitudes and longitudes were digitized for georeferencing. From this we constructed a mapping so that any digitized curve could be converted to latitude and longitude coordinates.

We digitized the boundary of each shaded patch (of constant ice concentration) within each study region, as illustrated in Fig. 2 (coloured lines). Each type of shading has high and low estimates of the ice concentration. We computed the area of each digitized patch, multiplied by the high and low ice concentration estimates, and added together all the contributions within a study region to get high and low estimates of the total ice area in that region.

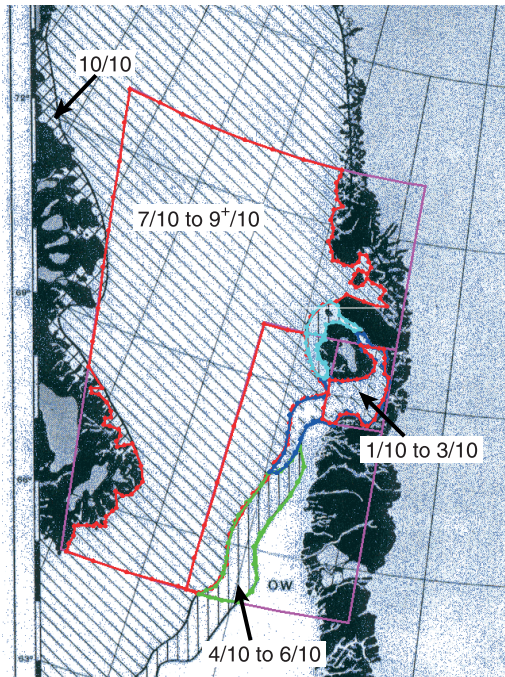


Fig 2. Sample chart from the Danish Meteorological Institute for March 1979 showing the sea ice concentration in Baffin Bay/Davis Strait (grey striped areas). Greenland is on the right, Baffin Island is on the left (as in Fig. 1). The charts indicate ice concentrations of 10/10 (cross-hatching), 7/10 to 9⁺/10 (diagonal stripes), 4/10 to 6/10 (vertical stripes), 1/10 to 3/10 (diagonal dashes), and less than 1/10 (no shading). We digitized areas of constant ice concentration lying within the study regions (coloured lines). For example, the green lines outline an area within the medium study region whose ice concentration is between 4/10 and 6/10.

Construction of time series

Our goal is to construct a consistent time series of the ice area in March in each study region for 1953 to 2001. The main task is to reconcile the chart data with the satellite data during the period of overlap, 1979–1981.

Figure 3 shows four separate time series, covering different time intervals, of the ice area in March in each study region. We make the following observations about the chart estimates and the satellite estimates during the three years of overlap: (1) In the large region the high chart estimate differs from the satellite estimate by -4% (1979), -6% (1980) and -1% (1981). (2) In the medium region the differences are 0% , -12% and $+12\%$. (3) In the small region the differences

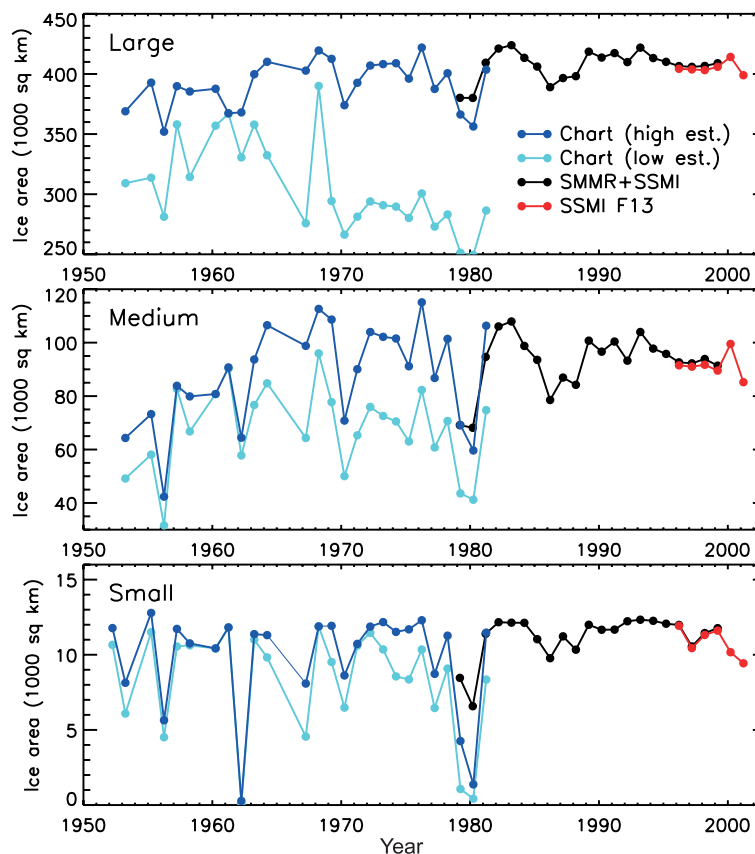
are -50% , -79% and $+1\%$. (4) The low chart estimates are substantially below the satellite estimates in all cases. The high chart estimates are in reasonably good agreement with the satellite estimates in the medium and large study regions. The agreement is not good in the small study region. This may just be due to sampling variability associated with a small region, or possibly due to land contamination of the satellite data at coastal pixels that contain a mix of ocean and land—the small study region has a relatively large number of pixels adjacent to land. Another factor is the large number of icebergs discharged into Disko Bay that may register as sea ice in the satellite data but not in the chart data.

Based on the comparison of chart and satellite estimates above, we use the high chart estimate as the best approximation for the construction of a consistent time series of ice area. Any weighted average of the high and low chart estimates would worsen the agreement with the satellite estimates during 1979–1981. Furthermore, giving weight to the low estimate would increase the trend in ice area from the chart period to the satellite period (see Fig. 3). To have the most conservative estimate of the increasing trend in sea ice, we use the high chart estimate and give zero weight to the low chart estimate. We can only speculate as to why the high chart estimate should give the best approximation to the satellite data. Perhaps human observers on ships and aircraft preferentially sample areas of lower ice concentration. Also, when one is estimating a quantity that is near its upper limit of 100%, there is greater potential to underestimate than to overestimate.

Since the chart data for 1952–56 are from April, not March, we applied an adjustment to account for the (typically) larger ice area in March. Using the satellite-derived ice areas for March and April, 1979–1999, we computed the median amount by which the March area exceeds the April area. (The median is insensitive to outliers.) Values for the small, medium and large study regions are, respectively, 500 km^2 , 12300 km^2 and 14100 km^2 . These values were added to the chart-derived ice areas for 1952–56.

As noted previously, NSIDC distributes two data sets of monthly sea ice concentration from passive microwave data for the post-1995 period, which we denote by “SMMR+SSMI” (1978–1999) and “SSMI F13” (1995–present). During the period of overlap, both data sets are based

Fig 3. Time series of ice area (thousands of km²) in March in the three study regions. The dark blue and light blue lines are the high and low estimates, respectively, derived from the chart data. The black and red lines are from passive microwave satellite data, as indicated in the top panel. The high chart estimate is in reasonable agreement with the satellite estimate during the years of overlap (1979–1981) for the large and medium study regions.



on the same underlying data from the SSMI instrument on the DMSP F13 satellite, and both use the Bootstrap algorithm to derive sea ice concentration. We compared the data sets for March 1996–1999 in the three study regions (see Fig. 3). The SMMR+SSMI ice concentration is consistently larger than the SSMI F13 ice concentration, with average differences of 0.66%, 1.7% and 1.0% in the large, medium and small regions, respectively. These differences, which we consider negligible, are likely due to small differences in the implementation of the Bootstrap algorithm.

To summarize the construction of the final time series in each study region: we use the high chart estimate for 1952–1978 (small region) or 1953–1978 (medium and large regions), with adjustments for 1952–56 as described above; the SMMR+SSMI satellite estimates for 1979–1995; and the SSMI F13 estimates for 1996–2001. Years with missing data are 1954, 1959, 1965 and 1966.

Analysis of trends

For each study region we fit a line to the time series constructed in the previous section, using a standard least squares procedure. (For the small study region we excluded the year 1962 because of its anomalously low ice area: 276 km².) We computed the standard deviation of the slope of each line using the formula

$$\sigma_{slope} = \frac{\sigma_{residuals}}{\sigma_{years} \times \sqrt{n-2}}$$

where $\sigma_{residuals}$ is the standard deviation of the residuals of the least squares fit, n is the number of years in the time series, and σ_{years} is the standard deviation of the years. We also computed the significance of the slope using a standard F test with 1 and $n-2$ degrees of freedom (Draper & Smith 1998). By significance we mean the confidence level (%) with which the null hypothesis of zero slope is rejected. Results are shown in Table

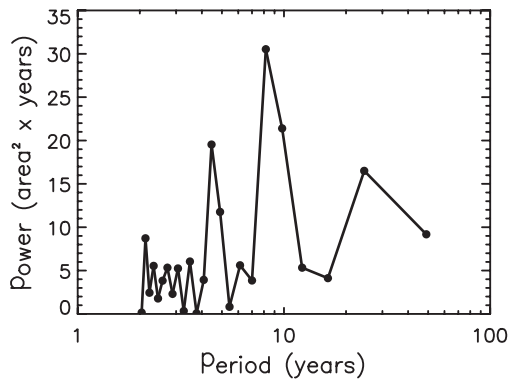


Fig 4. Power spectrum of the time series of ice area in the large study region. The trend in the time series was first removed; no filters were used. The peak is at a period of 8.2 years. The unit of area is 1000 km².

1. The slope of ice area vs. time for the large study region is 3.7 standard deviations above zero, a solid positive trend with a significance of 99.9%. The medium study region also shows a convincing positive trend with a significance of 93%. The ice area in the small region has an increasing trend but with less certainty. Trends during the satellite period alone (1979–2001) for the large, medium, and small study regions are (in %/decade) 1.0, 3.5 and 4.5, respectively. Although the chart data and satellite data were collected by very different means and there is some uncertainty in their cross-calibration, comparison with Table 1 shows that the trends during the satellite period are not radically different from the trends over the entire 49-year record.

The oscillatory character of the ice area in the medium and large study regions is at least as apparent as the increasing trends (see Fig. 3). A decadal cycle is evident with low points in 1962, 1970, 1979, 1986 and 1997. The power spectrum for the large region (Fig. 4) has a peak at a period of 8.2 years. Parkinson (1995) noted an apparent period of 6–7 years for the sea ice extent in Baffin Bay and Davis Strait, based on passive microwave data from 1978–1991. She cautioned against attributing long-term trends to behaviour that has a large cyclic component. The trends are sensitive to the period of record, as pointed out again by Parkinson et al. (1999). Their record of wintertime sea ice extent began in 1979, a particularly low ice year in Baffin Bay, which explains the relatively large trend over the period 1979–1996.

Discussion

We have constructed time series of sea ice area in March in three study regions of West Greenland for 1953–2001, using digitized chart data (1953–1978) from DMI and satellite data (1979–2001). Walsh & Johnson (1979) constructed an Arctic-wide data set of monthly sea ice concentration on a 110-km grid using, in part, data from DMI from 1957 onwards. Our data set is different in that we focus on specific regions of West Greenland and use the chart data in its full detail rather than at a set of grid points.

We find significant increasing trends in sea ice in our large and medium study regions, with substantial decadal variability superimposed. The increase in sea ice is likely to affect the biological productivity in the area by delaying the primary production and reducing the transport of energy up through the food web. Growth and survival of fish larvae will ultimately be affected, with possible effects for the fisheries as well. Large concentrations of sea birds along West Greenland utilize the openings in the sea ice for accessing the bottom on the shallow banks (Merkel et al. 2002), and several species of marine mammals use leads and cracks in the sea ice for breathing (Heide-Jørgensen & Acquarone 2002). Increasing sea ice is potentially lethal to animals that depend on these openings (Heide-Jørgensen et al. 2002).

The strength of the NAO and the location of its low-pressure centre have a major impact on ice conditions on the Atlantic side of the Arctic Ocean and sub-Arctic seas. Hilmer & Jung (2000) noted an eastward shift in the winter NAO's centre of variability around 1978, coincidentally just at the start of the satellite record of ice concentration. Indeed, we find the correlation of NAO and ice area in the large study

Table 1. For the time series of ice area in each region: slope of the least squares line \pm standard deviation (km²/yr); slope in terms of % per decade; and significance (%) of slope from F test.

Region	Slope \pm SD km ² /yr	Slope %/decade	Sig. %
Large	542 \pm 146	1.4	99.9
Medium	256 \pm 137	2.8	93
Small	16 \pm 17	1.5	66

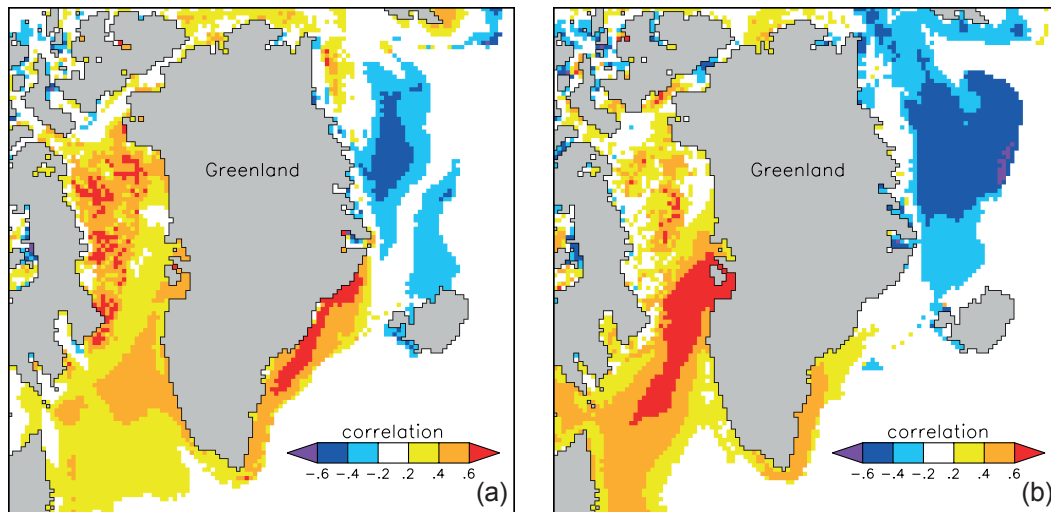


Fig 5. (a) Correlation of winter (December–March) sea ice concentration from SMMR+SSMI (1979–1999) with winter NAO index (1979–1999). (b) Correlation of sea ice concentration (1979–1999) with the *previous* winter's NAO index (1978–1998).

region is 0.09 for 1953–1978 but 0.60 for 1979–2001. Mysak et al. (1996) showed that heavy ice years in Baffin Bay and the Labrador Sea were associated with strong NAO and ENSO (El Niño – Southern Oscillation) events, which occurred in 1972–73, 1982–83 and 1991–92. Our pixel-by-pixel correlation map of the winter (December–March) sea ice concentration from SMMR+SSMI (1979–1999) with the winter NAO index (Fig. 5a) shows a dipole pattern with high correlation in Baffin Bay and low correlation in the Greenland Sea. A high NAO (strong Icelandic low pressure system) tends to bring cold air and higher sea ice concentration to Baffin Bay. Correlations on the order of 0.3 are seen in a broad region from Davis Strait to the coast of Labrador. However, the correlations with the *previous* winter's NAO index are on the order of 0.7 for the same region (Fig. 5b). This suggests that next year's ice conditions in West Greenland can be predicted to some extent by this winter's NAO index. The NAO predictor is better than persistence—the autocorrelation of sea ice area in the large study region is 0.44 at a lag of one year.

Further study is underway to examine the pattern of ice edge changes in Baffin Bay–Davis Strait and assess its biological impact.

Acknowledgements.—We thank the Danish Cooperation for the Environment in the Arctic for funding this study. We thank Henrik Steen Andersen at the Danish Meteorological Institute for providing ice charts. The satellite-derived sea ice concentration data are from the National Snow and Ice Data Center in Boulder, CO. We thank two anonymous reviewers for helpful comments.

References

- Comiso, J. C. 1995: *SSM/I concentrations using the bootstrap algorithm*. NASA Report 1380.
- Deser, C., Walsh, J. E. & Timlin, M. S. 2000: Arctic sea ice variability in the context of recent atmospheric circulation trends. *J. Clim.* 13, 617–633.
- Draper, N. R. & Smith, H. 1998: *Applied regression analysis*. New York: John Wiley & Sons.
- EWG (Environmental Working Group Joint U.S. Russian Sea Ice Atlas) 2000: *Sea ice atlas for the Arctic Ocean. Version 1.0, 1 September 2000*. Boulder, CO: National Snow and Ice Data Center.
- Heide-Jørgensen, M. P. & Acquarone, M. 2002: Size and trends of the bowhead, beluga and narwhal stocks wintering off West Greenland. *Scientific Publications of the North Atlantic Marine Mammal Commission* 4, 191–210.
- Heide-Jørgensen, M. P., Richard, P., Ramsay, M. & Akeegagok, S. 2002: Three recent ice entrapments of Arctic cetaceans in West Greenland and the eastern Canadian high Arctic. *Scientific Publications of the North Atlantic Marine Mammal Commission* 4, 143–148.
- Hilmer, M. & Jung, T. 2000: Evidence for a recent change in the link between the North Atlantic Oscillation and Arctic sea ice export. *Geophys. Res. Lett.* 27, 989–992.

- Hurrell, J. W. 1995: Decadal trends in the North Atlantic Oscillation: regional temperatures and precipitation. *Science* 269, 676–679.
- Melling, H., Gratton, Y. & Ingram, G. 2001: Ocean circulation within the North Water Polynya of Baffin Bay. *Atmos.–Ocean* 39, 301–325.
- Merkel, F. R., Mosbech, A., Boertmann, D. & Grøndahl, L. 2002: Winter seabird distribution and abundance off southwestern Greenland, 1999. *Polar Res.* 21, 17–36.
- Mysak, L. A., Ingram, R. G., Wang, J. & van der Baaren, A. 1996: The anomalous sea-ice extent in Hudson Bay, Baffin Bay and the Labrador Sea during three simultaneous NAO and ENSO episodes. *Atmos.–Ocean* 34, 313–343.
- Parkinson, C. L. 1995: Recent sea-ice advances in Baffin Bay/Davis Strait and retreats in the Bellingshausen Sea. *Ann. Glaciol.* 21, 348–352.
- Parkinson, C. L., Cavalieri, D. J., Gloersen, P., Zwally, H. J. & Comiso, J. C. 1999: Arctic sea ice extents, areas, and trends, 1978–1996. *J. Geophys. Res.* 104(C9), 20837–20856.
- Rigor, I. G., Colony, R. L. & Martin, S. 2000: Variations in surface air temperature observations in the Arctic, 1979–97. *J. Clim.* 13, 896–914.
- Walsh, J. E. & Johnson, C. M. 1979: An analysis of Arctic sea ice fluctuations, 1953–77. *J. Phys. Oceanogr.* 9, 580–591.